Obesity and brain topological organization differences throughout the lifespan.

Ottino-González, J.[1,2,3,*], **Baggio, H.C.**[2,4,*], **Jurado, M.A.**[1,2,3,✉], **Segura, B.**[2,4], **Caldú, X.**[1,2,3], **Prats-Soteras, X.**[1,2,3], **Tor, C.**[7], **Sender-Palacios, M.J.**[7], **Miró, N.**[6], **Sánchez-Garre, C.**[6], **Dadar, M.**[5], **Dagher, A.**[5], **García-García, I.**[5], **and Garolera, M.**[8,9]

[1]Departament de Psicologia Clínica i Psicobiologia. Universitat de Barcelona, Spain.
[2]Institut de Neurociències. Universitat de Barcelona, Spain.
[3]Institut de Recerca Sant Joan de Dèu. Hospital Sant Joan de Dèu, Spain.
[4]Departament de Medicina. Universitat de Barcelona, Spain.
[5]Montreal Neurological Institute. McGill University, Canada.
[6]Unitat de Endocrinologia, Hospital de Terrassa. Consorci Sanitari de Terrassa, Spain.
[7]CAP Terrassa Nord. Consorci Sanitari de Terrassa, Spain.
[8]Unitat de Neuropsicologia, Hospital de Terrassa. Consorci Sanitari de Terrassa, Spain.
[9]Brain, Cognition and Behaviour Research Group. Consorci Sanitari de Terrassa, Spain.
[*]These authors contributed equally to this work.

Abstract – Life expectancy and obesity rates have drastically increased in recent years. An unhealthy weight is related to long-lasting biological deregulations that might compromise the normal course of development and jeopardize the so-called "successful aging". The aim of the current study was to test whether an obesity status could mimic the functional organization of an otherwise healthy aged brain. Thus, the current study included adults with (N = 32, mean age 34.5 ± 6.49) and without obesity (N = 34, mean age 32.7 ± 6.79) as well as adolescents with obesity (N = 30, mean age 15.3 ± 2.64) and normal-weight (N = 31, mean age 15.6 ± 2.60). A sample of stroke-free non-obese and non-demented seniors was also entered (N = 32, mean age 66.1 ± 7.43). Participants underwent resting-state MRI acquisition and graph-based measurements of segregation, integration and robustness (i.e., mean degree and strength) were calculated. Obesity in adults was followed by a broad pattern of loses in robustness when compared to healthy-weight adults and seniors, as well as increases in network segregation relative to elders. Differences in adolescents followed the same direction yet they did not survive multiple comparison adjustment. No interaction emerged when exploring the transition from childhood to adulthood accounting for body-weight status. Altogether, and yet more research is needed, an obesity status could negatively render network resilience and compromise the normal course of aging.

Obesity | Aging | Maturation | Resting-state | Graph-theory
Correspondence: ***majurado@ub.edu***

Introduction

Our life expectancy is longer than it has ever been before. Above 30% of the population from Western developed countries will be older than 60 years by 2050 (World Health Organization, 2015). For this reason, research on the psychobiological factors that have an impact on the so-called "successful aging" is rapidly gaining popularity. One of such factors is obesity. The World Health Organization (WHO) estimates that the prevalence of obesity has tripled in the last decades (WHO, 2017). Particularly, children and teenagers with obesity represent a serious matter of concern as they are most likely to stay overweight throughout life and develop cardiometabolic comorbidities earlier than adults (WHO, 2018). The far-reaching consequences of obesity involve several chronic conditions, such as type II diabetes, cardiovascular diseases and cancer (Wade, Carslake, Sattar, Davey Smith, & Timpson, 2018). On a similar note, obesity could accelerate brain aging (Ronan et al., 2016; Tzanetakou, Katsilambros, Benetos, Mikhailidis, & Perrea, 2012), increasing the odds of suffering late-onset dementia, such as Alzheimer's disease and vascular dementia (Bischof & Park, 2015). The neurobiological mechanisms behind this, however, remain largely elusive. Neuroanatomical studies suggest that obesity is associated with reductions in gray matter (GM) volume (García-García et al., 2018) and alterations in white matter (WM) microstructure (Repple et al., 2018; Zhang et al., 2018). Likewise, yet to a lesser extent, changes within these tissues were also reported in younger individuals (Kennedy, Collins, & Luciana, 2016; Ou, Andres, Pivik, Cleves, & Badger, 2015). Thus, morphologically at least, an obesity status could induce premature changes in the brain that resemble those prompted by aging.

The functional organization of the brain is intricate. Distinct and anatomically distant regions interact with each other contributing to cognitive function. Graph-based indexes could serve as proxies of the complex rendering of large-scale networks. Measures of segregation, such as modularity, represent how neighboring nodes tend to aggregate as independent clusters (Rubinov & Sporns, 2010). This community-based organization underpins the principle of brain economics where modules specialize onto processing certain sources of information, principally those of sensory nature (Wig, 2017). Integration indexes reflect instead to which extent a priori unrelated modules interchange information. A typical surrogate of integration is the characteristic path length (path length, from now on). This parameter reflects the shortest path between modules (Rubinov & Sporns, 2010). Hence, the fewer the jumps, the greater the integration between communities. Well-balanced short and long-range connections allow the rapid combination of resources necessary for higher cognitive activity. Finally, degree and strength mirror the network integrity and efficiency by averaging the amount and the weight of connections a given node has with

DRAFT

the rest of the brain (Rubinov & Sporns, 2010). Densely interconnected nodes are metabolically costly and commonly referred to as "hubs" as they exert as bridges coupling remote clusters (van den Heuvel & Sporns, 2013).

Aging is associated with losses in the differentiation between well-defined circuits. In older adults, nodes that once belonged to independent clusters tend to enhance their between-cluster communications at the expense of their within-cluster interactions. In other words, aging is associated with decreases in modularity (Geerligs, Renken, Saliasi, Maurits, & Lorist, 2015) and increases in path length (Sun, Tong, & Yang, 2012). These losses in network discreteness could expose either the recruitment of age-related compensatory mechanisms (Geerligs et al., 2015), the decreases in the number of nodes and short-range connections (i.e., drops in network integrity and efficiency) (Sala-Llonch et al., 2014), or both. Similarly, during childhood and adolescence, the developing brain progressively steps from highly clustered and randomly wired communities towards less modular and better connected ones (Boersma et al., 2013). These are thought to reflect age-related changes in GM/WM tissue (i.e., axonal pruning, cell-shrinkage) (Cao et al., 2014).

To date, and to the best of our knowledge, only four studies have explored the brain functional organization in obese individuals with graph-theoretical parameters, three of them in adults. Two of them reported lower modularity in individuals with obesity when compared to healthy-weight subjects (Baek, Morris, Kundu, & Voon, 2017; Chao et al., 2018). The third and fourth study described global brain connectivity decreases mainly within prefrontal circuits in both adults and adolescents (Geha, Cecchi, Todd Constable, Abdallah, & Small, 2017; Moreno-Lopez, Contreras-Rodriguez, Soriano-Mas, Stamatakis, & Verdejo-Garcia, 2016). Because of its long-term consequences over health, and the suggestion that it might accelerate the normal course of aging, the current study had two aims. The first and main objective was to compare the brain connectivity organization of adults with and without obesity to otherwise healthy elders. The second aim was to examine whether an obesity status could differently shape the brain topological organization during maturation, or the transition from childhood to adulthood.

Methods

Participants. Two independently collected samples were included in this work. One sample comprised 32 non-obese healthy seniors (51-85 years old). The recruitment procedure of this group is fully described in Abós et al. (2017). Briefly, exclusion criteria consisted on presence of psychiatric or neurological comorbidity, low global intelligence quotient estimated by the WAIS-III Vocabulary subtest score (> 7 scalar score) (Wechsler, 1999), and a Mini-Mental state examination score below 25 (Folstein, Folstein, & McHugh, 1975). For the current work, senior participants with obesity (body mass index [BMI] equal to or higher than 30 kg/m^2) were excluded (N = 4) as well as those presenting MRI pathological findings such as white matter hyperintensities unrelated to the course of normal aging (N = 2).

The other sample included 61 adolescents (12-21 years old) and 66 adults (22-48 years old) from public health care centers belonging to the *Consorci Sanitari de Terrassa*. This sample was recruited in the context of a broader line of research revolving around obesity and brain function. Part of this sample was used in previous works (Ariza et al., 2012; Caldú et al., 2019; García-García et al., 2013a, 2013b, 2013c, 2015; Marqués-Iturria et al., 2013, 2014, 2015; Ottino-González et al., 2017, 2018, 2019). Thirty-two adults were considered as obese and 34 as normal weight (BMI < 24.9 kg/m^2). Following the cut-offs established by the WHO (2012), 30 adolescents above the gender-based 95th BMI percentile were categorized as obese, and 31 teens oscillating between the 5th and the 84th percentile, were categorized as healthy-weight (Cole, Flegal, Nicholls, & Jackson, 2007). Thirty-four individuals with overweight (i.e., BMI 25 kg/m^2 to 29.9 kg/m2^2, or between the 85th and 94th percentiles for adolescents) were not included in this study since we were only interested in addressing the two extremes of the BMI continuum.

As in previous work, we excluded participants with cardiometabolic comorbidities (i.e., type II diabetes, hypercholesterolemia, hypertension), as well as those with past or present neurological or psychiatric disorders. Individuals underwent three visits. The first consisted of a fasting blood sample extraction and a medical exploration. The second visit included an extensive neuropsychological evaluation in which subjects with a Vocabulary subtest scalar score below 7 were discarded (WAIS-III or WISC-IV) (Wechsler, 1999, 2007). The third and last visit comprised a magnetic resonance imaging (MRI) acquisition at the *Hospital Clínic de Barcelona*.

Additionally, participants from all five groups exhibiting excessive head motion were discarded (N = 16). Excessive movement was defined as (1) mean interframe head motion greater than 0.3 mm translation or 0.3° rotation, and (2) maximum interframe head motion greater than 1 mm translation or 1° rotation.

MRI acquisition. Images were acquired with a 3T Siemens scanner (MAGNETOM Trio, Siemens, Germany). Each participant underwent a T1-weighted structural image for co-registration and parcellation purposes with the MPRAGE-3D protocol [echo time (TE) = 2.98 ms; repetition time (TR) = 2300 ms; inversion time = 900 ms; 256 mm field of view [FOV]; matrix size = 256 x 256; voxel size = 1.0 x 1.0 x 1.0 mm^3). Resting-state volumes in adolescents and adults were collected using a multi-slice gradient-echo EPI sequence covering the whole brain (TE = 19 ms; TR = 2000 ms; 3 mm slice thickness; 90° flip angle; 220 mm FOV; voxel size = 1.7 x 1.7 x 3.0 mm^3). Resting-state images in the elders were obtained with the following parameters: TE = 28 ms, TR = 2500 ms, 3 mm slice thickness, 80° flip angle, 240 mm FOV, voxel size = 1.7 x 1.7 x 3.0 mm^3.

Image pre-processing. Basic functional image preprocessing, using AFNI (http://afni.nimh.nih.gov/afni) and FSL (https://www.fmrib.ox.ac.uk/fsl) tools, included: discarding

DRAFT

the first five volumes to allow magnetization stabilization, despiking, motion correction, brain extraction, grand-mean scaling, linear detrending, and high-pass filtering (maintaining frequencies above 0.01 Hz). Functional images and T1-weighted volumes were co-registered and then non-linearly normalized to the MNI ICBM152 template. Then, images were non-linearly transformed to MNI space at 3 x 3 x 3 mm^3 voxel size using SPM (http://www.fil.ion.ucl.ac.uk/spm/).

To remove the effects of head motion and other non-neural sources of signal variation from the functional data sets, we used an independent component analysis (ICA)-based strategy for Automatic Removal of Motion Artifacts (ICA-AROMA) (Pruim et al., 2015). This method uses individual resting-state data to perform ICAs and automatically identify artifact-related independent components. The time courses of components considered as artifactual were stored to be used as regressors during network computation.

The six motion parameters obtained from the realignment procedure, as well as the average white matter and cerebrospinal fluid signals were kept as regressors in network reconstruction. To generate the corresponding white matter and cerebrospinal fluid (lateral ventricle) masks, T1-weighted structural images were segmented using FreeSurfer (https://surfer.nmr.mgh.harvard.edu/). The resulting binary masks were linearly transformed from structural to native functional space using FSL-FLIRT (https://fsl.fmrib.ox.ac.uk/fsl/fslwiki/FLIRT). To prevent these masks from extending to the adjacent gray matter due to resampling blur in linear transformation, white matter masks were then "eroded" by applying a threshold of 0.9, while ventricular masks were thresholded at 0.3.

Connectivity matrix computation. To reconstruct the functional connectome, the brain needs to be divided into a set of nodes; network edges connecting pairs of nodes are then defined as a measure of relationship between their respective time courses. In this work, we used the Brainnetome atlas (Fan et al., 2016), a cross-validated connectivity-based parcellation scheme that divides the cerebrum into 210 cortical and 36 subcortical gray matter regions, taken as network nodes. The first eigenvariates of the time series of all voxels included in each region mask were extracted using *fslmeants* and taken as the time course of the corresponding nodes.

Individual 246 x 246 connectivity matrices were then reconstructed by calculating the standardized regression coefficient between the time courses of nodes *i* and *j*, while also entering the ICA-AROMA artifact time courses, six motion parameters, and white matter and cerebrospinal fluid mean time courses as regressors. This produces fully connected and undirected brain networks with 30,135 unique edges with values ranging between -1 and 1.

Moreover, a group temporal-concatenation spatial ICA was performed using FSL's MELODIC (https://fsl.fmrib.ox.ac.uk/fsl/fslwiki/MELODIC) with a pre-determined dimensionality of 15 independent components. The spatial and power spectral characteristics of the resulting components were inspected to identify 10 well-established networks (Griffanti et al., 2017): two primary visual networks (PVN and PVN2), secondary visual network (SVN), default mode network (DMN), dorsal attentional network (DAN), anterior default mode network (aDMN), right and left frontoparietal networks (FPN), sensory-motor network (SM) and the salience network (SN) (see Supplementary Figure 1). Two additional networks were identified as the medial temporal network (MTN) (including the hippocampus and the amygdala) and the striatal-thalamic network (STN).

These data-driven spatial maps were used to assign the Brainnetome's nodes to specific brain networks for further regional graph-based measurements calculation, using in-house MATLAB scripts. Specifically, the Z-maps generated by MELODIC corresponding to the 12 networks of interest were thresholded at $Z \geq 2$. Subsequently, each Brainnetome node was considered to belong to a network if over 60% of its voxels overlapped with this network's thresholded map. When this overlap occurred for more than one network, the sum of the Z-values across all overlapping voxels was considered, and the node was assigned to the network with the highest Z-value sum. In total, 153 of the 246 Brainnetome nodes were ascribed to one of the 12 networks of interest, as shown in Supplementary Table 1.

Global and regional measurements estimation. Global network parameters were computed using the Brain Connectivity Toolbox (Rubinov & Sporns, 2010) and in-house MATLAB scripts. As non-normalized global parameters, the modularity coefficient was estimated using the Louvain algorithm and indicating the degree to which a network can be subdivided into well-defined modules with few intermodular connections.

Normalized weighted global measures were computed by averaging the ratio between the actual measure and those obtained through randomly rewiring the connectivity matrix 500 times using a degree-preserving algorithm. Thus, after setting negative edge weights to zero, we computed the characteristic path length, defined as the average minimum number of edges that need to be traversed between each pair of network nodes (Rubinov & Sporns, 2010).

We also assessed other two complementary non-normalized metrics: the mean network degree (i.e., average number of positive connections linked to a node, across all brain nodes) and the mean network strength (i.e., average of unthresholded connection strength across all edges, positive and negative), both of which can be understood as measures of network efficiency and integrity, or robustness. Regional parameters such as nodal degree and strength were calculated by averaging the total number of connections and weights between nodes ascribed to each ICA-based network and the rest of the brain.

Statistical analysis

Sociodemographic variables as well as the mean interframe translational and rotational movements of the head were examined across groups. Non-parametrical tests were applied when data assumptions were violated. All comparisons, including post-hoc pairwise contrasts, of global and regional

DRAFT

graph-based measures were conducted with permutation-based tests (10,000 permutations). One-factor univariate general linear models (GLMs) were conducted in adults and seniors. To avoid comparisons of non-interest, differences in adolescents were tested in independent models. Post-hoc pairwise t-tests were performed for contrasts that emerged as statistically significant. Cumulative odds for false-positive results were prevented with Bonferroni-adjustments. Here, the raw p-values were multiplied by *k* variables for omnibus tests (i.e., by 4 for global graph-based measures, and by 12 for regional degree and strength parameters), and by *n* contrast of interest (i.e., adults with obesity vs. healthy-weight adults, adults with obesity vs. seniors and healthy-weight adults vs. seniors) in post-hoc comparisons. Statistical significance was set at adjusted p-value < 0.05. Likewise, effect sizes (i.e., Cohen's d) and bias-corrected and accelerated bootstrap (10,000 simulations) confidence intervals (CI) at 95% were calculated for each significant pairwise contrast. Moreover, to explore for differences in the transition from young to adulthood in both global and regional graph-related indexes, we sought for interactions between body-weight status (i.e., healthy-weight vs. obesity) and age (i.e., adolescent vs. adult) with two-factor univariate GLMs. All statistical analyses were performed with *R* version 3.5.0 (R Core Team, 2018).

Results

Sociodemographics. As expected, groups differed in age ($F_{(4,153)}$ = 420, p < 0.001) and years of education ($F_{(4,153)}$ = 24.62 p < 0.001). Post-hoc tests revealed no significant differences between adults with and without obesity in age (p-adjusted = 0.674) or education (p-adjusted = 0.854). Similarly, healthy-weight and obese adolescents were comparable in terms of age (p-adjusted = 0.999) and years of education (p-adjusted = 0.732). All five groups were equally distributed for sex (x^2 = 1.22, p = 0.875) (Table 1).

Table 1. Sociodemographics across groups (mean and standard deviation)

Groups	Age	Education	N/Females
OB adult	34.53 (6.49)	13.88 (2.92)	32/20
HW adult	32.68 (6.79)	14.62 (2.75)	34/18
Senior	66.13 (7.43)	11.22 (4.26)	32/17
OB young	15.27 (2.64)	8.57 (2.45)	30/15
HW young	15.64 (2.60)	9.52 (2.19)	31/16

OB = participant with obesity, HW = healthy-weight individual.

MRI quality check. Rotational movements of the head did not diverge between groups ($H_{(4)}$ = 4.32, p = 0.364). By contrast, head translational movements did prove different ($H_{(4)}$ = 38.90, p < 0.001). Post-hoc contrasts revealed that such displacements were more marked for elders and adults with obesity, as both of them differed from the other groups yet not from each other. Consequently, head translational movements were controlled for all further graph-theoretical analyses including these groups, either by introducing it as a covariate or by regressing out its effects from the variable of interest.

Global graph-based results. Adults and seniors exhibited differences in modularity ($F_{(3,94)}$ = 5.71, p-adjusted = 0.020), mean degree ($F_{(3,94)}$ = 5.56, p-adjusted = 0.024), and mean strength ($F_{(3,94)}$ = 4.81, p-adjusted = 0.039).

Post-hoc tests exposed that the contrast between adults with obesity and without did not pass the Bonferroni adjustment (raw p-value = 0.024). Still, individuals with obesity showed lower mean degree (t = 2.69, p-adjusted = 0.012, d = -0.66; CI_{bca}95% [-1.11, -0.19]) and mean strength (t = 2.74, p-adjusted = 0.015, d = -0.68; CI_{bca}95% [-1.10, -0.21]) when compared to their normal-weight counterparts. Relative to seniors, adults with obesity presented greater modularity (t = -3.94, p-adjusted = 0.002, d = 0.99; CI_{bca}95% [0.45, 1.55]), as well as lower mean degree (t = 3.38 , p-adjusted = 0.007, d = -0.85; CI_{bca}95% [-1.32, -0.37]) and strength (t = 2.81, p-adjusted = 0.025, d = -0.70; CI_{bca}95% [-1.16, -0.22]). Normal-weight adults did not differ from non-obese elders for any of the abovementioned. Results are depicted below in Figure 1.

While analogous to adults, differences in adolescents in mean degree and strength did not survive multiple comparison correction (0.034 and 0.033, raw p-values for each contrast) (see Figure 3 and Figure 4). Additionally, mean and standard deviation across groups for graph-based parameters are included in the Supplementary Table 2.

Regional nodal degree and strength results. Adults and seniors diverged in the average number of inward and outward connections in the DMN ($F_{(3,94)}$ = 5.97, p-adjusted = 0.048). Here, adults with obesity displayed lesser regional degree than healthy-weight adults in the DMN (t = 3.21, p-adjusted = 0.008, d = -0.79; CI_{bca}95% [-1.26 -0.33]) and seniors(t = 3.15, p-adjusted = 0.007, d = -0.79; CI_{bca}95% [-1.26 -0.28]).

Groups also diverged in the DMN strength connectivity ($F_{(3,94)}$ = 7.02, p-adjusted = 0.022). Adults with obesity demonstrated lower strength when rivalled against their healthy-weight peers (t = 3.67, p-adjusted = 0.001, d = -0.90; CI_{bca}95% [-1.33, -0.44]) and non-obese elders (t = 2.57, p-adjusted = 0.031, d = -0.64; CI_{bca}95% [-1.03, -0.17]). Healthy-weight adults did not prove different from seniors neither for degree nor strength in the DMN (see Figure 3).

What is more, differences in the regional degree ($F_{(3,94)}$ = 6.61, p-adjusted = 0.008) emerged in the SMN. In contrast to healthy-weight adults, adults with obesity revealed lesser nodal degree (t = 3.45, p-adjusted = 0.005, d = -0.85; CI_{bca}95% [-1.35, -0.36]). The contrast from adults with obesity and elders did not survive Bonferroni adjustment (raw p-value = 0.041). Groups also differed in the SMN strength ($F_{(3,94)}$ = 6.23, p-adjusted = 0.031). Adults with obesity did also show lesser strength than healthy-weight adults within this network (t = 3.54, p-adjusted = 0.002, d = -0.87; CI_{bca}95% [-1.37, -0.38]). The contrast between this group and elders did not emerge as statistically significant. Adults

DRAFT

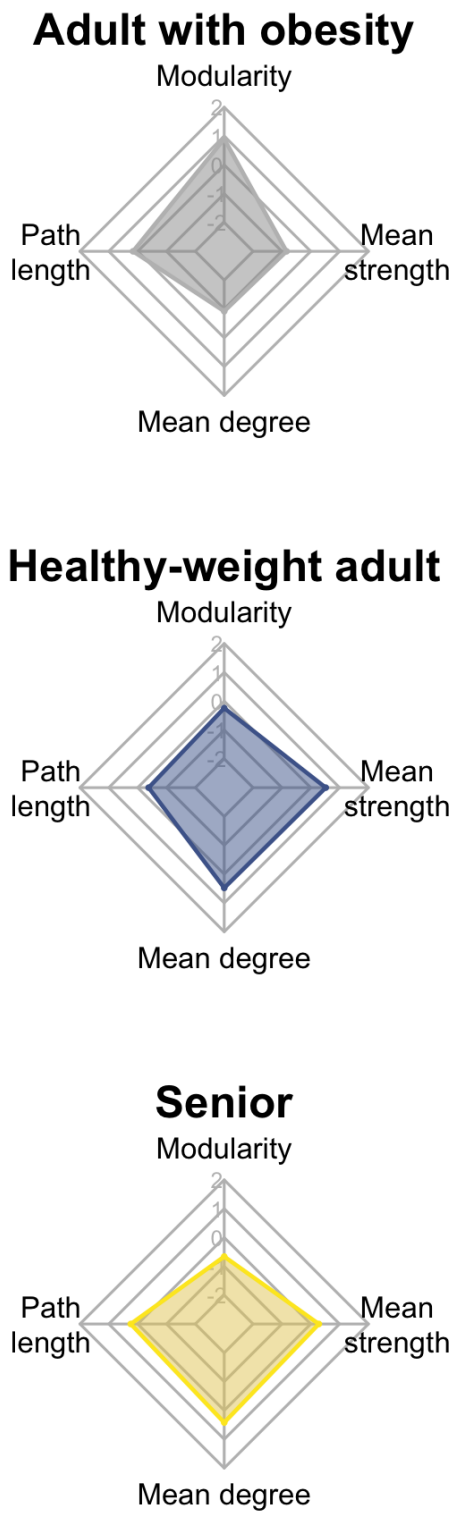

Figure 1. Network profiles of adults with obesity, healthy-weight adults and seniors.

without obesity did not differ from seniors for any measure of the SMN. Results are displayed in Figure 4.

Adolescents with and without obesity only proved different in the regional degree (t = 2.98, p-adjusted = 0.043, d = -0.76;

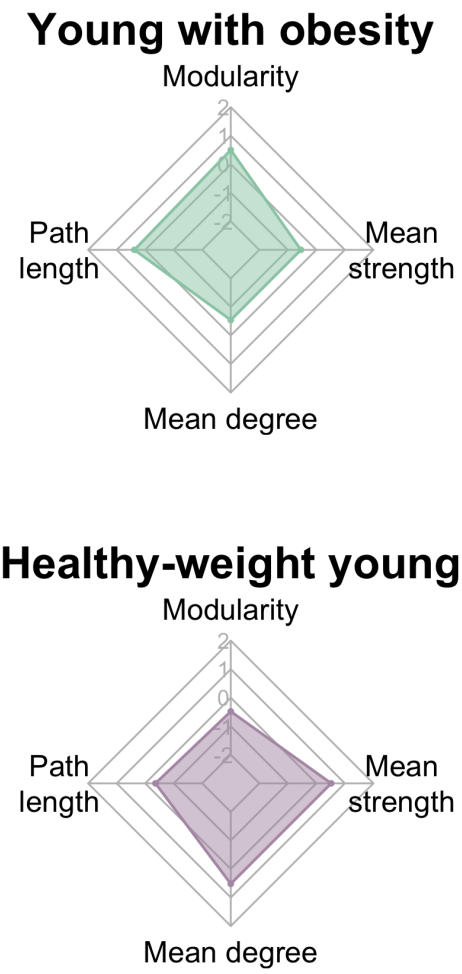

Figure 2. Network profiles of adolescents with and without obesity.

CI_{bca}95% [-1.27 -0.24]) and strength (t = 3.10, p-adjusted = 0.041, d = -0.79; CI_{bca}95% [-1.31 -0.24]) of the PVN (see Figure 5).

Body-weight status and age interaction. There were no significant interactions between body-weight status and age for any graph-theoretical measurement as presented in Figure 6. No interaction emerged for regional indexes either.

Discussion

Obesity is a preventable health problem associated with the development of long-lasting cardiometabolic disorders (Wade et al., 2018) and late-onset dementia (Bischof & Park, 2015; Deckers, van Boxtel, Verhey, & Köhler, 2017). The current work aimed to shed a broader light on whether an obesity status could relate to differences in how large-scale networks are rendered at two relevant time windows: senescence and maturation. Adults with obesity demonstrated greater modularity in comparison to non-obese seniors. Moreover, this group also exhibited lower mean degree and strength when compared to healthy-weight adults

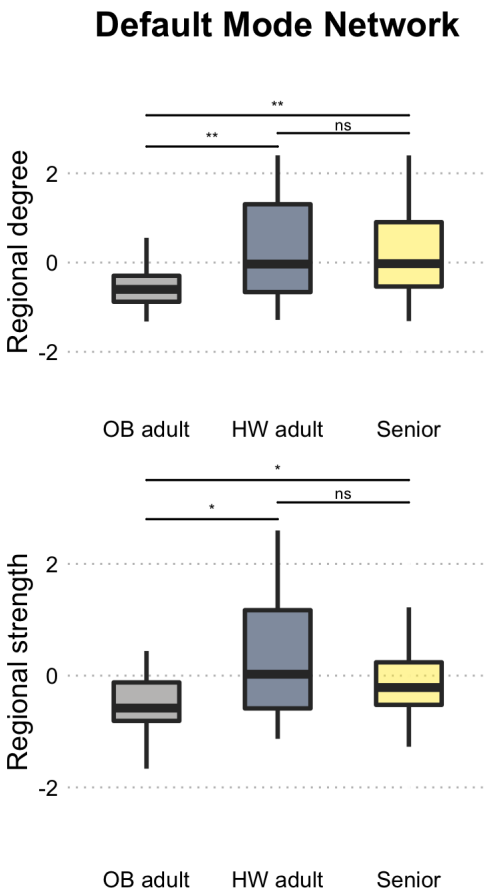

Figure 3. Group comparison for DMN regional degree and strength. OB = participants with obesity, HW = healthy-weight individuals, *<0.05, **<0.01, ns = non-significant.

and non-obese elders. These results did partially stand in line with our hypothesis of an obesity status mimicking an aged brain. This pattern of increased segregation and lesser robustness could represent a drawback for successful aging in the future, which is further discussed. Strikingly, normal-weight adults did not diverge from seniors for any graph-theoretical parameter. Moreover, and despite contrasts in adolescents for global measurements did not survive multiple comparison, youngsters did show differences in the regional properties of visual-related networks. Lack of results in global-based parameters will be disclosed separately for this group. Finally, no interaction emerged as significant between body-weight status and age for any of the abovementioned.

Modularity. This index can be generally regarded as a proxy of network segregation, which stands for how clustered the brain is in terms of sharing and processing information (Sporns, 2013). As the brain ages, modularity tends to decrease (Cao et al., 2014). This is the result of the progressive scattering of intra-network pairwise connections (Geerligs et al., 2015; Sala-Llonch, Bartrés-Faz, & Junqué, 2015; Sala-Llonch et al., 2014). Adults with obesity showed a pattern of enhanced cliquishness relative to seniors (and healthy-weight adults to some extent) with relatively large effect sizes. This, however, was contrary to what was originally hypothesized. An increase in such parameter reflects that the information is densely handled within clusters rather than be generally distributed, which is the opposite scenario to be occurring in the elderly. Although this could benefit the processing of sensory-specific information, higher-level cognitive activity may in turn deteriorate from this particular rendering (Sporns, 2013). Excessively isolated clusters would not be able to exchange information efficiently. This may relate to the well-known increment in the processing times and background noise that elders and subjects with obesity are lean to show in their cognitive performance (Deckers et al., 2017; Sala-Llonch et al., 2014). Also, an escalation in modularity could entail a vulnerability to cardiovascular-related disconnection syndromes (e.g., aphasia) (Siegel et al., 2018).

Global and regional mean degree and strength. These parameters, respectively, echo the number of edges connected to a given node and the average weight of such links. Therefore, both return a global reading of the network integrity and efficiency, or robustness. Our results showed that adults with obesity presented a lower mean degree and strength when compared to healthy-weight adults with effect sizes ranging from medium to large. These results are partially in line with the study conducted by Geha et al. (2017). In this work, the authors served a measure of global brain connectivity, defined as the number of connections each node has with others. Moreover, one of the consequences of aging on the brain is

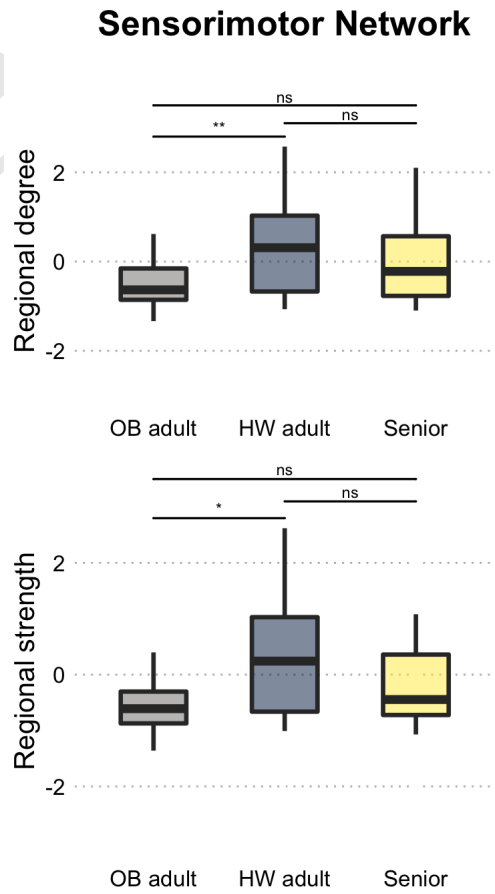

Figure 4. Group comparison for SMN regional degree and strength. OB = participants with obesity, HW = healthy-weight individuals, *<0.05, **<0.01, ns = non-significant.

DRAFT

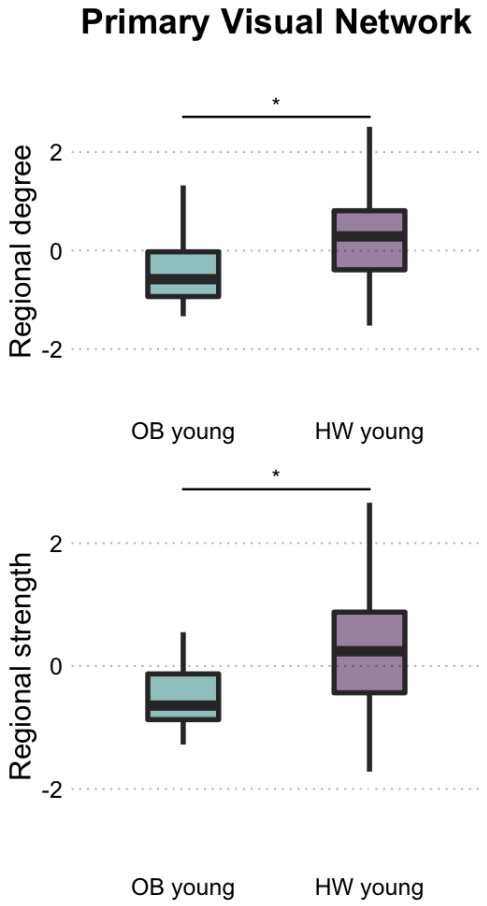

Figure 5. Group comparison for PVN regional degree and strength. OB = participants with obesity, HW = healthy-weight individuals, *<0.05.

the trimming of short-range edges and the scattering of nodes (Sala-Llonch et al., 2014). Individuals with obesity did show loses in overall network robustness, a result that did support our hypothesis. The increase in network fragility could in turn be echoing symptoms of premature aging (Geerligs et al., 2015; Sala-Llonch et al., 2015, 2014). What is more, when examined regionally, we found group differences in sensory-driven (i.e., SMN) and task-negative networks (i.e., DMN), which support our previous findings suggesting reductions in whole-brain network-resilience. Also, adolescents with obesity presented lower degree and strength in primary-visual networks (i.e., PVN). Sensory-processing circuits (e.g., SMN and PVN), are naturally engaged during the handling of domain-specific information. Subjects with obesity feature alterations within tactile and visual-processing networks (Doucet et al., 2017; García-García et al., 2013; Geha et al., 2017). The DMN, the most typical task-negative network, is considered to be a biomarker for pathological aging and dementia (Buckner, Andrews-Hanna, & Schacter, 2008; Palmqvist et al., 2017). This network is also extremely vulnerable to the negative effects of obesity-related disorders such as type II diabetes (Wang, Ji, Lu, & Zhang, 2016), hypertension (Haight et al., 2015), and dyslipidemia (Spielberg et al., 2017). To date, very few studies have described alterations in the DMN relative to an obesity status (Beyer et al., 2017; Doucet et al., 2017; Figley, Asem, Levenbaum, & Courtney, 2016; Tregellas et al., 2011).

Interestingly, no meaningful differences were found among healthy-weight adults and seniors. Literature is consistent in describing modularity reductions in elders (Geerligs et al., 2015; Song et al., 2014), a finding that we failed to replicate as both groups showed similar scores. Equally, decreases in robustness neither emerged as significant for this particular contrast. It is important to remark, however, that none of the participants in the senior group presented obesity, a condition that alone (Beyer et al., 2017; Doucet et al., 2017), or in conjunction with its medical complications (Haight et al., 2015; Spielberg et al., 2017; Wang et al., 2016), is enough to yield differences in network connectivity. This criterion is often overlooked in healthy-aging literature. Following this line, the group of elders used in this work was composed by literate individuals, free from stroke and cognitively intact. Although more research is needed, we cannot rule out the possibility that this sample might not have been representative of their population. Therefore, some of the results hereby presented should be taken with caution.

Similarly, differences in adolescents with and without obesity did not survive multiple comparison correction for global indexes. It is likely that group differences would have passed such threshold with an enough-powered sample size (or, obviously, with a less-restrictive one). On another note, the body-weight status did not seem to influence the transition from childhood to adulthood as originally assumed. Intriguingly, adolescents and adults with obesity followed the same pattern of network-weakening in comparison to their healthy-weight counterparts. Differences in metrics aside, evidence of loses in network robustness is documented in a recent

DRAFT

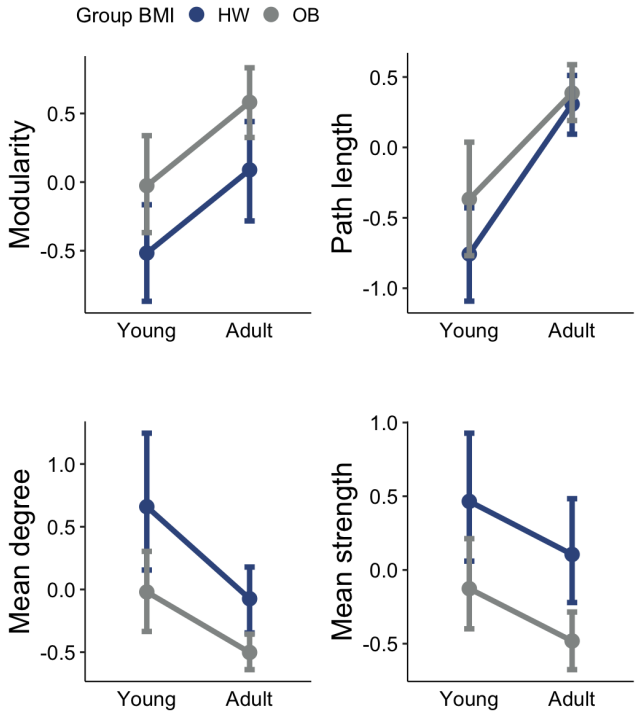

Figure 6. Age and body-weight status interactions for global graph-related indexes. OB = participants with obesity, HW = healthy-weight individuals.

work conducted in adolescents (Moreno-Lopez et al., 2016). Hence, the functional alterations here noted in adults with obesity might already be noticeable at early developmental stages. Still, this inference, as preliminary as it is, should be properly confirmed with longitudinal studies.

In line with the earlier exposed, the current work has limitations that should be addressed in the future. First, the study cross-sectional nature represents a pitfall as concluding upon the causality of the results here presented is extremely discouraged. Longitudinal approaches would help disentangle whether the transition from childhood to adulthood and to elderhood is different in the presence of an unhealthy weight. Second, our modest sample size (N = 159) might have limited our statistical power to catch any subtle disparity between groups (i.e., adolescents with and without obesity contrasts). Third, to have had a group of elders with obesity would have allowed exploring the impact of such condition across all possible age ranges. Fourth, the resting-state acquisition in the senior cohort were slightly distinct from the rest of the groups. Particularly, the echo-time was different in this group, which might have resulted in differences in BOLD signal sensitivity. Thus, further works should try comparing groups with equal MRI acquisition parameters. By contrast, a strong point of this work was the strict criteria that ruled out participants with neurological or psychiatric comorbidities likely prompting differences in network properties.

In sum, compared to non-obese seniors, volunteers with obesity exhibited increases in network segregation. Relative to healthy-weight adults and elders, this group revealed reductions in network robustness. Overall, an obesity status represents an avoidable flaw that proved negatively render network resilience in this group. Although more research is needed, this scenario might compromise the normal course of aging in individuals with obesity.

Bibliography

1. A. Abós, H Baggio, B. Segura, A.I. García-Díaz, Y. Compta, M.J. Martí, F. Valldeoriola, and C. Junqué. Discriminating cognitive status in Parkinson's disease through functional connectomics and machine learning. *Scientific Reports*, 7(1):45347, 12 2017. ISSN 2045-2322. doi: 10.1038/srep45347.
2. M. Ariza, M. Garolera, M.A. Jurado, I. Garcia-Garcia, I. Hernan, C. Sánchez-Garre, M. Vernet-Vernet, M.J. Sender-Palacios, I. Marques-Iturria, R. Pueyo, B. Segura, and A. Narberhaus. Dopamine Genes (DRD2/ANKK1-TaqA1 and DRD4-7R) and Executive Function: Their Interaction with Obesity. *PLoS ONE*, 7(7):e41482, 1 2012. ISSN 1932-6203; 1932-6203. doi: 10.1371/journal.pone.0041482.
3. K. Baek, L. S. Morris, P. Kundu, and V. Voon. Disrupted resting-state brain network properties in obesity: Decreased global and putaminal cortico-striatal network efficiency. *Psychological Medicine*, 47(4):585–596, 2017. ISSN 14698978. doi: 10.1017/S0033291716002646.
4. F. Beyer, S. Kharabian Masouleh, J.M. Huntenburg, L. Lampe, T. Luck, S.G. Riedel-Heller, M. Loeffler, M.L. Schroeter, M. Stumvoll, A. Villringer, and A.V. Witte. Higher body mass index is associated with reduced posterior default mode connectivity in older adults. *Human Brain Mapping*, 3515(April):3502–3515, 2017. ISSN 10970193. doi: 10.1002/hbm.23605.
5. G.N. Bischof and D.C. Park. Obesity and Aging. *Psychosomatic Medicine*, 77(6):697–709, 1 2015. ISSN 0033-3174. doi: 10.1097/PSY.0000000000000212.
6. M. Boersma, D.J.A. Smit, D.I. Boomsma, E.J.C. De Geus, H.A. Delemarre-van de Waal, and C.J. Stam. Growing Trees in Child Brains: Graph Theoretical Analysis of Electroencephalography-Derived Minimum Spanning Tree in 5- and 7-Year-Old Children Reflects Brain Maturation. *Brain Connectivity*, 3(1):50–60, feb 2013. ISSN 2158-0014. doi: 10.1089/brain.2012.0106.
7. R.L. Buckner, J.R. Andrews-Hanna, and D.L. Schacter. The brain's default network: Anatomy, function, and relevance to disease. *Annals of the New York Academy of Sciences*, 1124:1–38, 2008. ISSN 00778923. doi: 10.1196/annals.1440.011.
8. X. Caldú, J. Ottino-González, C. Sánchez-Garre, I. Hernan, E. Tor, M.J. Sender-Palacios, J.C. Dreher, M. Garolera, and M.A. Jurado. Effect of the catechol- O -methyltransferase Val 158 Met polymorphism on theory of mind in obesity. *European Eating Disorders Review*, (August 2018):1–9, 2 2019. ISSN 10724133. doi: 10.1002/erv.2665.
9. S.H. Chao, Y.T. Liao, V.C.H. Chen, C.J. Li, R.S. McIntyre, Y. Lee, and J.C. Weng. Correlation between brain circuit segregation and obesity. *Behavioural Brain Research*, 337(259):218–227, 2018. ISSN 18727549. doi: 10.1016/j.bbr.2017.09.017.
10. T.J Cole, K.M Flegal, S. Nicholls, and A.A Jackson. Body mass index cut offs to define thinness in children and adolescents: international survey. *BMJ (Clinical research ed.)*, 335 (7612):194, 7 2007. ISSN 1468-5833. doi: 10.1136/bmj.39238.399444.55.
11. G.E. Doucet, N. Rasgon, B.S. McEwen, N. Micali, and S. Frangou. Elevated Body Mass Index is Associated with Increased Integration and Reduced Cohesion of Sensory-Driven and Internally Guided Resting-State Functional Brain Networks. *Cerebral Cortex*, (April): 988–997, 2017. ISSN 1047-3211. doi: 10.1093/cercor/bhx008.
12. M.S. Ellulu, I. Patimah, H. Khaza'ai, A. Rahmat, and Y. Abed. Obesity and inflammation: the linking mechanism and the complications. *Archives of Medical Science*, 4:851–863, 2017. ISSN 1734-1922. doi: 10.5114/aoms.2016.58928.
13. L. Fan, H. Li, J. Zhuo, Y. Zhang, J. Wang, L. Chen, Z. Yang, C. Chu, S. Xie, A.R. Laird, P.T. Fox, S.B. Eickhoff, C. Yu, and T. Jiang. The Human Brainnetome Atlas: A New Brain Atlas Based on Connectional Architecture. *Cerebral Cortex*, 26(8):3508–3526, 8 2016. ISSN 1047-3211. doi: 10.1093/cercor/bhw157.
14. C.R. Figley, J.S.A. Asem, E.L. Levenbaum, and S.M. Courtney. Effects of body mass index and body fat percent on default mode, executive control, and salience network structure and function. *Frontiers in Neuroscience*, 10(June):1–23, 2016. ISSN 1662-453X. doi: 10.3389/fnins.2016.00234.
15. M.F. Folstein, S.E. Folstein, and P.R. McHugh. "Mini-mental state": A practical method for grading the cognitive state of patients for the clinician. *Journal of Psychiatric Research*, 12 (3):189–198, 11 1975. ISSN 00223956. doi: 10.1016/0022-3956(75)90026-6.
16. D. Frasca, B.B. Blomberg, and R. Paganelli. Aging, obesity, and inflammatory age-related diseases. *Frontiers in Immunology*, 8(DEC):1–10, 2017. ISSN 16643224. doi: 10.3389/fimmu.2017.01745.
17. I. García-García, A. Narberhaus, I. Marqués-Iturria, M. Garolera, A. Rădoi, B. Segura, R. Pueyo, M. Ariza, and M. A. Jurado. Neural Responses to Visual Food Cues: Insights from Functional Magnetic Resonance Imaging. *European Eating Disorders Review*, 21(2): 89–98, 3 2013. ISSN 10724133. doi: 10.1002/erv.2216.
18. I. García-García, M.A. Jurado, M Garolera, B Segura, I Marqués-Iturria, R Pueyo, M Vernet-Vernet, M.J. Sender-Palacios, R Sala-Llonch, M Ariza, A Narberhaus, and C Junqué. Functional connectivity in obesity during reward processing. *NeuroImage*, 66:232–239, 2 2013. ISSN 10538119. doi: 10.1016/j.neuroimage.2012.10.035.
19. I. García-García, M.A. Jurado, M. Garolera, B. Segura, R. Sala-Llonch, I. Marqués-Iturria, R. Pueyo, M.J. Sender-Palacios, M. Vernet-Vernet, A. Narberhaus, M. Ariza, and C. Junqué. Alterations of the salience network in obesity: A resting-state fMRI study. *Human Brain Mapping*, 34(11):2786–2797, 11 2013. ISSN 10659471. doi: 10.1002/hbm.22104.
20. I. García-García, M.A. Jurado, M. Garolera, I. Marqués-Iturria, A. Horstmann, B. Segura, R. Pueyo, M.J. Sender-Palacios, M. Vernet-Vernet, A. Villringer, C. Junqué, D.S. Margulies, and J. Neumann. Functional network centrality in obesity: A resting-state and task fMRI study. *Psychiatry Research: Neuroimaging*, 233(3):331–338, 9 2015. ISSN 09254927. doi: 10.1016/j.pscychresns.2015.05.017.
21. I. García-García, A. Michaud, M. Dadar, Y. Zeighami, S. Neseliler, D.L Collins, A.C. Evans, and A. Dagher. Neuroanatomical differences in obesity: meta-analytic findings and their validation in an independent dataset. *International Journal of Obesity*, 9, 7 2018. ISSN 0307-0565. doi: 10.1038/s41366-018-0164-4.
22. L. Geerligs, R.J. Renken, E. Saliasi, N.M. Maurits, and M.M. Lorist. A Brain-Wide Study of Age-Related Changes in Functional Connectivity. *Cerebral Cortex*, 25(7):1987–1999, 7 2015. ISSN 1460-2199. doi: 10.1093/cercor/bhu012.
23. P. Geha, G. Cecchi, Todd C.R., C. Abdallah, and D.M. Small. Reorganization of brain connectivity in obesity. *Human Brain Mapping*, 38(3):1403–1420, 3 2017. ISSN 10659471. doi: 10.1002/hbm.23462.
24. L. Griffanti, G. Douaud, J. Bijsterbosch, S. Evangelisti, F. Alfaro-Almagro, M.F. Glasser, E.P. Duff, S. Fitzgibbon, R. Westphal, D. Carone, C.F. Beckmann, and S.M. Smith. Hand classification of fMRI ICA noise components. *NeuroImage*, 154(June 2016):188–205, 2017. ISSN 10959572. doi: 10.1016/j.neuroimage.2016.12.036.
25. I. Marqués-Iturria, R. Pueyo, M. Garolera, B. Segura, C. Junqué, I. García-García, M.J. Sender-Palacios, M. Vernet-Vernet, A. Narberhaus, M. Ariza, and M.A. Jurado. Frontal cortical thinning and subcortical volume reductions in early adulthood obesity. *Psychiatry Research: Neuroimaging*, 214(2):109–115, 11 2013. ISSN 09254927. doi: 10.1016/j.pscychresns.2013.06.004.
26. T.J. Haight, R.N. Bryan, G. Erus, C. Davatzikos, D.R. Jacobs, M. D'Esposito, C.E. Lewis, and L.J. Launer. Vascular risk factors, cerebrovascular reactivity, and the default-mode brain network. *NeuroImage*, 115:7–16, 2015. ISSN 10959572. doi: 10.1016/j.neuroimage.2015.04.039.
27. I. Marqués-Iturria, M. Garolera, R. Pueyo, B. Segura, I. Hernan, I. García-García, C. Sánchez-Garre, M. Vernet-Vernet, M.J. Sender-Palacios, A. Narberhaus, M. Ariza, C. Junqué, and M.A. Jurado. The interaction effect between BDNF val66met polymorphism and obesity on executive functions and frontal structure. *American Journal of Medical Genetics Part B: Neuropsychiatric Genetics*, 165(3):245–253, 4 2014. ISSN 15524841. doi: 10.1002/ajmg.b.32229.
28. I. Marqués-Iturria, L.H. Scholtens, M. Garolera, R. Pueyo, I. García-García, P. González-Tartiere, B. Segura, C. Junqué, M.J. Sender-Palacios, M. Vernet-Vernet, C. Sánchez-Garre, M.A. de Reus, M.A. Jurado, and M.P. van den Heuvel. Affected connectivity organization of the reward system structure in obesity. *NeuroImage*, 111:100–106, 5 2015. ISSN 10538119. doi: 10.1016/j.neuroimage.2015.02.012.
29. L. Moreno-Lopez, O. Contreras-Rodriguez, C. Soriano-Mas, E.A. Stamatakis, and A. Verdejo-Garcia. Disrupted functional connectivity in adolescent obesity. *NeuroImage: Clinical*, 12:262–268, feb 2016. ISSN 22131582. doi: 10.1016/j.nicl.2016.07.005.
30. J. Ottino-González, M.A. Jurado, I. García-García, X. Caldú, X. Prats-Soteras, E. Tor, M.J. Sender-Palacios, and M. Garolera. Allostatic load and executive functions in overweight adults. *Psychoneuroendocrinology*, 106(April):165–170, 8 2019. ISSN 03064530. doi: 10.1016/j.psyneuen.2019.04.009.
31. J. Ottino-González, M A Jurado, I. García-García, B Segura, I. Marqués-Iturria, M. J. Sender-Palacios, E. Tor, X. Prats-Soteras, X. Caldú, C. Junqué, O. Pasternak, and M. Garol-

DRAFT

era. Allostatic load and disordered white matter microstructure in overweight adults. *Scientific Reports*, 8(1):15898, 12 2018. ISSN 2045-2322. doi: 10.1038/s41598-018-34219-8.

32. J. Ottino-González, M.A. Jurado, I. García-García, B. Segura, I. Marqués-Iturria, M.J. Sender-Palacios, E. Tor, X. Prats-Soteras, X. Caldú, C. Junqué, and M. Garolera. Allostatic Load Is Linked to Cortical Thickness Changes Depending on Body-Weight Status. *Frontiers in Human Neuroscience*, 11(December):1–11, 12 2017. ISSN 1662-5161. doi: 10.3389/fnhum.2017.00639.
33. S. Palmqvist, M. Schöll, O. Strandberg, N. Mattsson, E. Stomrud, H. Zetterberg, K. Blennow, S. Landau, W. Jagust, and O. Hansson. Earliest accumulation of β-amyloid occurs within the default-mode network and concurrently affects brain connectivity. *Nature Communications*, 8(1):1214, 12 2017. ISSN 2041-1723. doi: 10.1038/s41467-017-01150-x.
34. R.H.R. Pruim, M. Mennes, D. van Rooij, A. Llera, J.K. Buitelaar, and C.F. Beckmann. ICA-AROMA: A robust ICA-based strategy for removing motion artifacts from fMRI data. *NeuroImage*, 112:267–277, 5 2015. ISSN 10538119. doi: 10.1016/j.neuroimage.2015.02.064.
35. R Core Team. R: A Language and Environment for Statistical Computing, 2018.
36. J. Repple, N. Opel, S. Meinert, R. Redlich, T. Hahn, N.R. Winter, C. Kaehler, D. Emden, R. Leenings, D. Grotegerd, D. Zaremba, Christian Bürger, Katharina Förster, Katharina Dohm, Verena Enneking, Elisabeth J. Leehr, Joscha Böhnlein, Greta Karliczek, Walter Heindel, Harald Kugel, J. Bauer, V. Arolt, and U. Dannlowski. Elevated body-mass index is associated with reduced white matter integrity in two large independent cohorts. *Psychoneuroendocrinology*, 91(March):179–185, 5 2018. ISSN 03064530. doi: 10.1016/j.psyneuen.2018.03.007.
37. L. Ronan, A.F. Alexander-Bloch, K. Wagstyl, S. Farooqi, C. Brayne, L.K. Tyler, Cam-CAN, P.C. Fletcher, Cam-CAN, and P.C. Fletcher. Obesity associated with increased brain age from midlife. *Neurobiology of aging*, 47:63–70, 7 2016. ISSN 1558-1497. doi: 10.1016/j.neurobiolaging.2016.07.010.
38. M. Rubinov and O. Sporns. Complex network measures of brain connectivity: Uses and interpretations. *NeuroImage*, 52(3):1059–1069, 9 2010. ISSN 10538119. doi: 10.1016/j.neuroimage.2009.10.003.
39. R. Sala-Llonch, C. Junqué, E.M. Arenaza-Urquijo, D. Vidal-Piñeiro, C. Valls-Pedret, E.M. Palacios, S. Domènech, A. Salvà, N. Bargalló, and D. Bartrés-Faz. Changes in whole-brain functional networks and memory performance in aging. *Neurobiology of Aging*, 35(10): 2193–2202, 10 2014. ISSN 01974580. doi: 10.1016/j.neurobiolaging.2014.04.007.
40. R. Sala-Llonch, D. Bartrés-Faz, and C. Junqué. Reorganization of brain networks in aging: a review of functional connectivity studies. *Frontiers in Psychology*, 6(May):1–11, 5 2015. ISSN 1664-1078. doi: 10.3389/fpsyg.2015.00663.
41. J.S. Siegel, B.A. Seitzman, L.E. Ramsey, M. Ortega, E.M. Gordon, N.U.F. Dosenbach, S.E. Petersen, G.L. Shulman, and M. Corbetta. Re-emergence of modular brain networks in stroke recovery. *Cortex*, 101:44–59, 2018. ISSN 19738102. doi: 10.1016/j.cortex.2017.12.019.
42. S.J. Spencer, H. D'Angelo, A. Soch, L.R. Watkins, S.F. Maier, and R.M. Barrientos. High-fat diet and aging interact to produce neuroinflammation and impair hippocampal- and amygdalar-dependent memory. *Neurobiology of Aging*, 58:88–101, 10 2017. ISSN 0197-4580. doi: 10.1016/J.NEUROBIOLAGING.2017.06.014.
43. J.M. Spielberg, N. Sadeh, E.C. Leritz, R.E. McGlinchey, W.P. Milberg, J.P. Hayes, and D.H. Salat. Higher serum cholesterol is associated with intensified age-related neural network decoupling and cognitive decline in early- to mid-life. *Human Brain Mapping*, 38(6):3249–3261, 2017. ISSN 10970193. doi: 10.1002/hbm.23587.
44. O Sporns. Network attributes for segregation and integration in the human brain. *Current opinion in neurobiology*, 1 2013. ISSN 1873-6882; 0959-4388. doi: 10.1016/j.conb.2012.11.015;10.1016/j.conb.2012.11.015.
45. O. Sporns. Structure and function of complex brain networks. *Dialogues in clinical neuroscience*, 15(3):247–262, 9 2013. ISSN 1958-5969.
46. J.R. Tregellas, K.P. Wylie, D.C. Rojas, J. Tanabe, J. Martin, E. Kronberg, D. Cordes, and M.A. Cornier. Altered Default Network Activity in Obesity. *Obesity (Silver Spring, Md.)*, 19 (21):2316–2321, 6 2011. ISSN 1930-7381; 1930-7381. doi: 10.1038/oby.2011.119.
47. I.P. Tzanetakou, N.L. Katsilambros, A. Benetos, D.P. Mikhailidis, and D.N. Perrea. "Is obesity linked to aging?": adipose tissue and the role of telomeres. *Ageing research reviews*, 11(2): 220–9, 5 2012. ISSN 1872-9649.
48. M.N. Valcarcel-Ares, Z. Tucsek, T. Kiss, C.B. Giles, S. Tarantini, A. Yabluchanskiy, P. Balasubramanian, T. Gautam, V. Galvan, P. Ballabh, A. Richardson, W.M. Freeman, J.D. Wren, F. Deak, Z. Ungvari, and A. Csiszar. Obesity in Aging Exacerbates Neuroinflammation, Dysregulating Synaptic Function-Related Genes and Altering Eicosanoid Synthesis in the Mouse Hippocampus: Potential Role in Impaired Synaptic Plasticity and Cognitive Decline. *The Journals of Gerontology: Series A*, 74(3):290–298, 2 2019. ISSN 1079-5006. doi: 10.1093/gerona/gly127.
49. M.P. van den Heuvel and O. Sporns. Network hubs in the human brain. *Trends in cognitive sciences*, 17(12):683–96, 12 2013. ISSN 1879-307X. doi: 10.1016/j.tics.2013.09.012.
50. K.H. Wade, D. Carslake, N. Sattar, S.G. Davey, and N.J. Timpson. BMI and Mortality in UK Biobank: Revised Estimates Using Mendelian Randomization. *Obesity*, 26(11):1796–1806, 11 2018. ISSN 1930-7381. doi: 10.1002/oby.22313.
51. D Wechsler. *WAIS III. Escala de Inteligencia de Wechsler para adultos III (adaptación española ed.)*, volume adaptación. TEA Editores S.A., Madrid, 1999.
52. D Wechsler. *WISC-IV: Escala de Inteligencia de Wechsler para Niños-IV (2da edición)*. Madrid, 2007.
53. G.S. Wig. Segregated Systems of Human Brain Networks. *Trends in Cognitive Sciences*, 21(12):981–996, 2017. ISSN 1879307X. doi: 10.1016/j.tics.2017.09.006.
54. World Health Organization. BMI classification, 2012.
55. World Health Organization. World Report on Ageing and Health. Technical report, 2015.
56. Regional Office for Europe World Health Organization. Obesity: Data and statistics. Technical report, 2017.
57. R. Zhang, F. Beyer, L. Lampe, T. Luck, S.G. Riedel-Heller, M. Loeffler, M.L. Schroeter, M. Stumvoll, A. Villringer, and A.V. Witte. White matter microstructural variability mediates the relation between obesity and cognition in healthy adults. *NeuroImage*, 172(February): 239–249, 2018. ISSN 10959572. doi: 10.1016/j.neuroimage.2018.01.028.

DRAFT

Supplementary Material

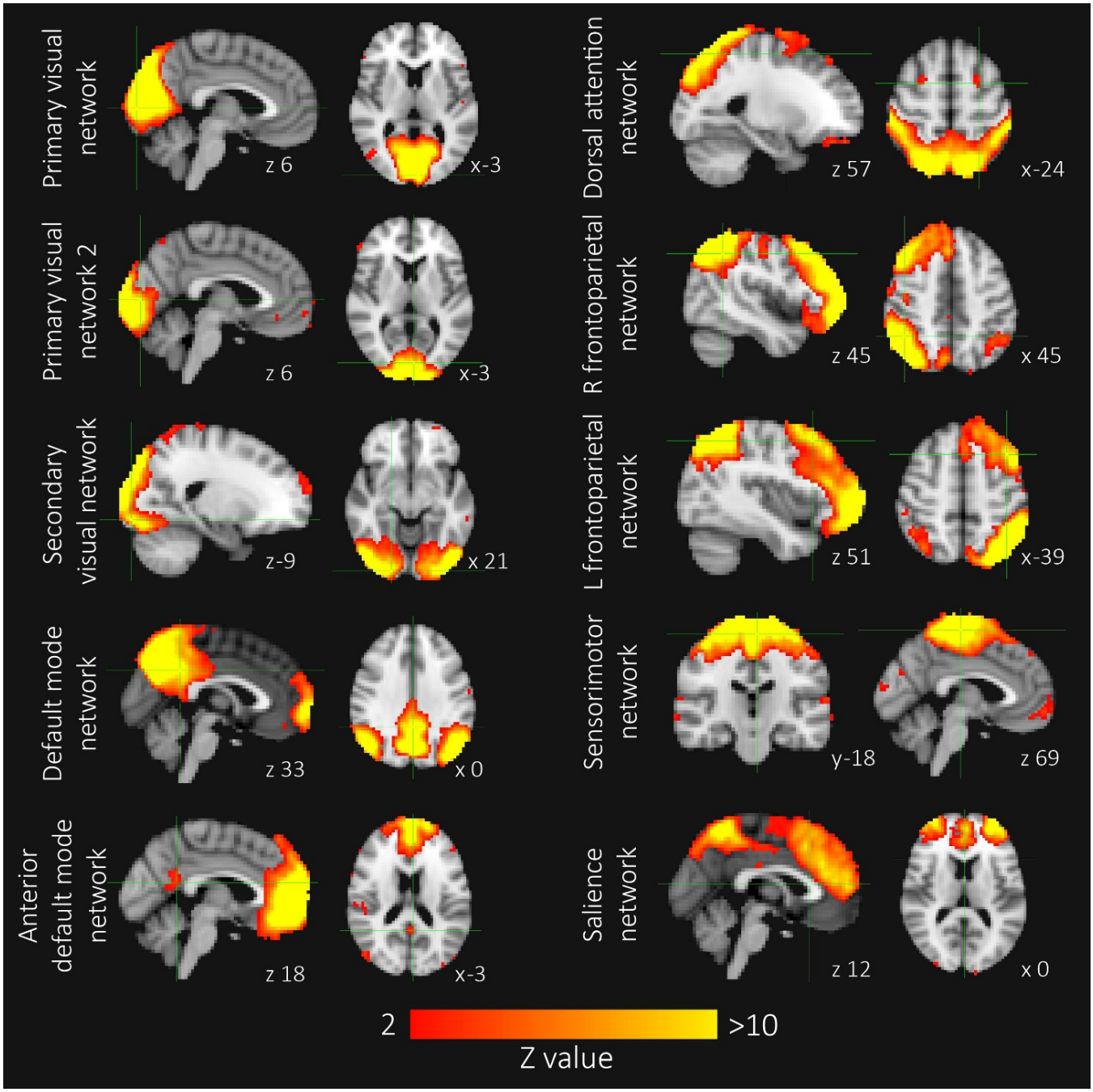

Supplementary Figure 1. Plots disclose the spatial maps corresponding to 10 networks of interest characterized through independent component analysis. The x, y or z MNI coordinates of the slices shown are indicated. In coronal and axial slices, the right hemisphere is displayed on the left side of the image. R: right; L: left.

Primary visual network					
Cun_L_5_2	Cun_L_5_4	Cun_L_5_5	Cun_R_5_2	Cun_R_5_3	Cun_R_5_5
sOcG_L_2_1	sOcG_R_2_1				
Primary visual network 2					
Cun_L_5_1	Cun_L_5_3	Cun_R_5_1	OcG_R_4_3		
Secondary visual network					
FuG_L_3_2	FuG_R_3_2	OcG_L_4_1	OcG_L_4_2	OcG_L_4_3	OcG_L_4_4
OcG_R_4_1	OcG_R_4_2	OcG_R_4_4	sOcG_L_2_2		
Anterior default mode network					
CG_L_7_7	CG_R_7_7	OrG_L_6_1	OrG_L_6_4	OrG_R_6_1	SFG_L_7_3
SFG_L_7_7	SFG_R_7_7				
Dorsal attention network					
IPL_L_6_1	IPL_R_6_1	IPL_R_6_3	ITG_L_7_5	ITG_R_7_2	ITG_R_7_5
sOcG_R_2_2	SPL_L_5_1	SPL_L_5_2	SPL_L_5_4	SPL_R_5_1	SPL_R_5_2
SPL_R_5_3	SPL_R_5_5				
Default mode network					
CG_L_7_1	CG_R_7_1	IPL_L_6_5	IPL_R_6_5	Pcun_L_4_1	Pcun_L_4_3
Pcun_L_4_4	Pcun_R_4_1	Pcun_R_4_3	Pcun_R_4_4	pSTS_L_2_2	
Left frontoparietal network					
IFG_L_6_1	IFG_L_6_2	IFG_L_6_3	IFG_L_6_4	IFG_L_6_6	IPL_L_6_2
ITG_L_7_2	ITG_L_7_6	MFG_L_7_2	MFG_L_7_4	MFG_L_7_5	MFG_L_7_6
OrG_L_6_2	OrG_L_6_3	OrG_L_6_6	SFG_L_7_2	SPL_L_5_5	
Right frontoparietal network					
IFG_R_6_2	IFG_R_6_3	IPL_R_6_2	ITG_R_7_6	MFG_R_7_4	MFG_R_7_5
MFG_R_7_6	MTG_R_4_1	OrG_R_6_2	OrG_R_6_3	OrG_R_6_6	SFG_R_7_2
SFG_R_7_3					
Salience network					
CG_L_7_3	CG_R_7_3	IPL_L_6_3	IPL_L_6_4	IPL_R_6_4	MFG_L_7_1
MFG_L_7_3	MFG_R_7_1	MFG_R_7_3	PCL_R_2_1	Pcun_L_4_2	SFG_L_7_1
SFG_L_7_6	SFG_R_7_1	SFG_R_7_6	SPL_L_5_3		
Sensorimotor network					
PCL_L_2_1	PCL_L_2_2	PCL_R_2_2	Pcun_R_4_2	PoG_L_4_4	PoG_R_4_4
PrG_L_6_3	PrG_L_6_4	PrG_R_6_2	PrG_R_6_3	PrG_R_6_4	SFG_L_7_4
SFG_L_7_5	SFG_R_7_4	SFG_R_7_5	SPL_R_5_4		
Medial temporal network					
Amyg_L_2_1	Amyg_L_2_2	Amyg_R_2_1	Amyg_R_2_2	Hipp_L_2_1	Hipp_L_2_2
Hipp_R_2_1	Hipp_R_2_2				
Striatal thalamic network					
Str_L_6_1	Str_L_6_2	Str_L_6_3	Str_L_6_4	Str_L_6_5	Str_L_6_6
Str_R_6_1	Str_R_6_2	Str_R_6_3	Str_R_6_4	Str_R_6_5	Str_R_6_6
Tha_L_8_1	Tha_L_8_2	Tha_L_8_3	Tha_L_8_4	Tha_L_8_5	Tha_L_8_6
Tha_L_8_7	Tha_L_8_8	Tha_R_8_1	Tha_R_8_2	Tha_R_8_3	Tha_R_8_4
Tha_R_8_5	Tha_R_8_6	Tha_R_8_7	Tha_R_8_8		

Supplementary Table 1. Brainnetome atlas regions (http://atlas.brainnetome.org/) assigned to each of the 12 brain networks of interest.

DRAFT

	OB adult	HW adult	Senior	OB young	HW young
Modularity	0.45 (0.80)	-0.12 (1.17)	-0.33 (0.82)	0.25 (0.99)	-0.24 (0.97)
Path length	0.08 (0.83)	-0.19 (0.85)	0.12 (1.27)	0.19 (1.04)	-0.18 (0.94)
Mean degree	-0.46 (0.65)	0.24 (1.17)	0.21 (0.96)	-0.27 (0.69)	0.26 (1.18)
Mean strength	-0.42 (0.67)	0.26 (1.18)	0.14 (0.96)	-0.27 (0.81)	0.26 (1.11)

Supplementary Table 2. Mean and standard deviation of graph-based parameters across groups (z-scores). OB = Participants with obesity, HW = Healthy-weight individuals.

DRAFT